

Extreme value statistics for North Atlantic cyclones

By FRANK SIENZ*, ANDREA SCHNEIDEREIT, RICHARD BLENDER, KLAUS FRAEDRICH and FRANK LUNKEIT, *Meteorologisches Institut, Universität Hamburg, Grindelberg 5, D-20144 Hamburg, Germany*

(Manuscript received 7 August 2009; in final form 18 March 2010)

ABSTRACT

Extremes of the cyclone intensity measures geopotential height (z_{1000}), mean horizontal gradient (∇z), cyclone depth (D), and relative vorticity (ζ_{850}), are analysed in re-analysis data (ERA40) and model simulations (ECHAM5/MPI-OM) in the North Atlantic region for extended winter seasons. Generalized Pareto distributions (GPD) are estimated for model validation and climate change assessment. Covariates, linear trend and North Atlantic Oscillation (NAO) are included to analyse the dependencies of the extremes.

In ERA40 no significant linear trend can be detected, while evidence for a NAO impact on z_{1000} , ∇z and ζ_{850} extremes is found. Model validation yields good agreement with consistent scale and shape, but a shift to lower values is notable. Like in ERA40 no trend is found in the simulation. The evidence for an NAO impact on cyclone extremes is less corroborated in the simulation, pointing to sample size effects.

In the warmer climate scenario (AIBS) extreme value statistics shows an intensification for all variables. Significant differences in GPD are obtained through testing for lower (higher) parameters. In contrast, considering all cyclones an increase is only present for z_{1000} , while a decrease is found for ∇z and ζ_{850} and no change for D .

1. Introduction

Extratropical cyclones are the major source of intra-annual climate variability in mid-latitudes. Huge damage is caused by intense storms and heavy precipitation associated with extraordinary intense baroclinic vortices. The growth and intensity of these vortices are determined by sea surface temperatures, baroclinicity and large-scale teleconnections (for example the North Atlantic Oscillation, NAO) which might be altered in an anthropogenic climate change (Pinto et al., 2009). Thus, the identification of possible changes of extratropical cyclone extremes is an important issue in the assessment of anthropogenic climate change.

The dominant mode of variability in the North Atlantic region is the NAO. During the strong positive phase of the NAO cyclone tracks tend to have a more northeastward orientation (Gulev et al., 2001). On the other hand, the variability of the NAO itself is substantially influenced by extratropical cyclones (Löptien and Ruprecht, 2005). However, the cyclone influence on the NAO typically occurs at different time scales (> 10 d) than the influence of the NAO to cyclone activity itself (Benedict et al., 2004). Furthermore, suitable growth conditions

for extreme cyclones occur in wider areas during the positive phase of the NAO (Pinto et al., 2009).

A common approach to investigate the characteristics of extratropical cyclones in large data sets is to determine individual cyclones, their tracks and their life cycles by using numerical detection and tracking algorithms. Various methods have been proposed and successfully applied to observations and model data for present day, palaeoclimate and anthropogenic climate change scenarios (for example Murray and Simmonds, 1991; Hodges, 1994; Blender et al., 1997). Evidence for anthropogenic changes in extratropical cyclone activity and characteristics is documented in many recent model studies (see Ulbrich et al., 2009 and references therein).

For the northern hemispheric winter the majority of scenario simulations show a slight decrease of the total number of cyclones (Bengtsson et al., 2009), while, on the other hand, there are hints that the number of intense cyclones increases (Lambert and Fyfe, 2006; defining intense cyclones as systems with core pressure less than 970 hPa). However, models do not agree with respect to these conclusions, in particular if individual regions are considered.

The definition of an extreme event and how its been analysed influences the results. In most studies, extreme cyclones are defined by a measure of their strength (e.g. the central pressure or the pressure gradient). A cyclone is considered extreme if its strength exceeds a subjectively chosen threshold or if it belongs

*Corresponding author.

e-mail: frank.sienz@zmaw.de

DOI: 10.1111/j.1600-0870.2010.00449.x

to upper percentiles of the distribution associated with intense cyclones.

Recently, the assessment of exceptional and rare events by extreme value statistics has become a widely used technique in the analysis of observational and model data (Katz et al., 2002; Kharin and Zwiers, 2005). Methods and concepts like, for example, the generalized extreme value (GEV) distribution, return values and statistical modelling based on maximum likelihood estimation in presence of covariates contribute substantially to the understanding of extreme events and to quantify potential changes of climate extremes due to anthropogenic forcing. An early application of extreme value statistics for extratropical cyclones is the work of Della-Marta and Pinto (2009). Here, their work is extended through analysing influences of linear trend and NAO. Further, detection of changes in cyclone parameters due to greenhouse gas warming are not restricted to return value analysis: additionally, the changes in the parameters of the GPD distributions are analysed.

The aim of this paper is to analyse the life cycles of intense extratropical cyclones using extreme value statistics. Using a detection and tracking algorithm individual cyclone tracks are extracted from re-analysis data and coupled model simulations for present-day (20th century) and a moderate greenhouse warming scenario (IPCC A1B). Extreme value statistics is applied to compare cyclone extremes simulated by the model with observations and to assess possible changes due to anthropogenic forcing. Furthermore, the relation between the extremes in cyclone parameters and the NAO are investigated. The analyses concentrate on the North Atlantic region during the extended Northern Hemispheric winter. In Section 2, the data used and the methodologies are introduced. The results are presented in Section 3. Conclusions, discussion and an outlook follows in Section 4.

2. Data and methods

North Atlantic/European cyclones are analysed in the re-analysis data of the European Center for Medium-Range Weather Forecasts (ERA40) and in simulations with the coupled atmosphere ocean model ECHAM5/MPI-OM. Extreme value statistics is applied to these data sets for extended winters (October–March). The relationships between extreme cyclone properties and the NAO are considered.

2.1. Data

The re-analysis encompasses the last half of the 20th century from September 1, 1957 to August 31, 2002 (Uppala et al., 2005). The data are computed at T159 spectral resolution on 60 vertical levels and stored with 6 hourly time steps. Here they are mapped to a spatial grid corresponding to T63 spectral resolution to enable an unbiased comparison with the model simulation.

The coupled atmosphere ocean model ECHAM5/MPI-OM uses an atmosphere with T63 spectral resolution on 31 vertical levels (Roeckner et al., 2003). The ocean MPI-OM model has a 1.5° resolution on 40 vertical levels (Marstrand et al., 2003). The coupling between atmosphere and ocean is implemented without flux corrections (Jungclaus et al., 2006). The data are available every 6 h. Three model experiments are analysed which are part of the IPCC contribution (for further details on the IPCC scenarios see Nakicenovic et al., 2000):

(i) *20C, 20th century*: The 20th century simulation (20C) for the period from 1957 to 2000 simulated with observed greenhouse gas concentrations, aerosols, and solar and volcanic forcing is compared with ERA40 re-analysis data.

(ii) *20CS stabilization*: After the year 2000, greenhouse gas concentrations are fixed at their 2000 level. This commitment experiment 20CS is analysed during the 2005–2100 period.

(iii) *A1BS stabilization*: To assess the potential impact of anthropogenic greenhouse forcing, the stabilization run of a A1B scenario is analysed. The A1B scenario describes a climate under gradual CO_2 increase from 2000 to 2100. A stabilization run extends this scenario with fixed greenhouse gas concentrations at the level of 2100. For one ensemble member of the A1B scenario, the stabilization run is extended about another 100 yr (2200–2300). To ensure the best stationarity, this extended stabilization time period is chosen for the analysis, beginning at 2205. However, the stabilization run of the 20th century (20C) ended in 2100. Therefore, the analysis is based on the stabilization run for the time period from 2005 to 2100.

The cyclone identification is based on the detection of minima in the 1000 hPa geopotential height field (Blender et al., 1997). To avoid erroneous detections, the cyclones must exist at least 2 d with a minimum mean horizontal gradient of 30 gpm/1000 km. The cyclones are identified in the Northern Hemisphere (20°N – 80°N) but the extreme value statistics is restricted to cyclones which attain an extremum in the North Atlantic sector (30°N – 80°N , 80°W – 40°E).

This study focuses on the following cyclone parameters: geopotential height in the centre of a cyclone (z_{1000}), mean horizontal gradient of the geopotential height in the neighbourhood (∇z), cyclone depth (D), all measured at 1000 hPa, and relative vorticity in the cyclone centre at 850hPa (ζ_{850}). z_{1000} and ζ_{850} are directly extracted from the data sets. ∇z is measured by the horizontal average of the calculated grid point gradients in a region corresponding to roughly 1000 km distance (Sickmüller et al., 2000). By fitting a Gaussian function to the cyclone centre and the surrounding height field, D is defined as the difference between a fitted environmental value and the geopotential height in the cyclone centre (i.e. D is positive). A description of this method is given in Schneidereit et al. (2010). These four quantities describe different physical meaning and spatial characteristics. Although z_{1000} characterizes the local geopotential height field at the cyclone centre, the variable D imply

information of the wider environment (roughly 1000 km). ∇z and ζ_{850} characterize the extratropical cyclone on the local scale in the cyclone centre. The dynamical characteristics ∇z and ζ_{850} are in close relationship. The extremum for each cyclone property (minima for z_{1000} , maxima for ∇z , D and ζ_{850}) during their individual cyclone life cycles is chosen for further analyses. For convenience, the signs for the z_{1000} minima are reversed to attain positive values for all variables considered.

EOF analysis is applied to monthly mean sea level pressure anomalies and used to determine the NAO by the leading principal component, in the region 20°N–80°N and 80°W–30°E. For ERA40 data the pressure field is interpolated to T63 resolution.

2.2. Extreme value statistics

There are two widely applied approaches to achieve extreme value distributions for identical and independent distributed random samples, X_1, X_2, \dots, X_n . One is based on division into blocks of the sample for which the block maxima are used to estimate the generalized extreme value distribution. The other method uses all data exceeding some well defined threshold, u . The resulting distribution function, for $y = X_i - u$ given $X_i > u$, is the generalized Pareto distribution (GPD):

$$H(y) = \begin{cases} 1 - \left(1 + \frac{\xi y}{\sigma}\right)^{-1/\xi}, & \text{for } \xi \neq 0 \\ 1 - \exp\left(-\frac{y}{\sigma}\right), & \text{for } \xi = 0 \end{cases} \quad (1)$$

with the parameters: scale, σ and shape, ξ . ξ determines the overall behaviour of the distribution. The three possible extremal types are: Fréchet $\xi > 0$, Gumbel $\xi = 0$ (achieved by taking the limit $\xi \rightarrow 0$), and Weibull $\xi < 0$. In this paper, the threshold method is applied because more values are incorporated into distribution estimation than with the block maxima approach. However, finding an optimal threshold, u is critical. Two graphical methods exist which are used in the following: the mean residual life plot and fitting over a range of thresholds (for details see Coles, 2003).

The estimated distributions are interpreted in terms of their return levels (quantiles), z_N , which are exceeded once every N years:

$$z_N = \begin{cases} u + \frac{\sigma}{\xi} \left[(N n_y k_u / n)^\xi - 1 \right], & \text{for } \xi \neq 0 \\ u + \sigma \log(N n_y k_u / n), & \text{for } \xi = 0 \end{cases} \quad (2)$$

n_y are the number of cyclones per year and the number of values exceeding u are given by k_u . Note that k_u/n is the estimate for the exceedance probability. Plotting z_N on a logarithmic scale gives return level plots guiding the decision which extremal type is present. That is, return level curves following a straight line result from Gumbel type distributions; the Fréchet (Weibull) type shows up with concave (convex) curves.

If data points and confidence intervals are included into the return level plots goodness of fit can be derived, which are performing well in the subsequent estimations. The confidence intervals

are calculated with profile-likelihood method (Coles, 2003) and enable also statements about the significance of return level differences. According to Kharin and Zwiers (2000) differences between two return levels are significant at the 1% level if their 90% confidence intervals do not overlap.

Cyclone life cycles are serial dependant, with increasing (decreasing) values before (after) an approached maximum. This will harm the independence assumption and affects the uncertainty analysis, so that confidence bounds are expected to be too narrow. Furthermore, GPD estimates on short time spans may be dominated by few strong and long-lasting cyclones. This problem is omitted by using one value, that is, the maximum during the cyclone life cycle. This is similar to standard declustering schemes but, for the problem at hand, the clusters are physically defined. Note that, beside serial dependant life-cycles, cyclone occurrences cluster in time (Mailier et al. 2006). This clustering may also hold for extreme cyclones, but is not considered in the following.

For observations and transient climate model simulations the extremes may potentially change in time. Such non-stationarities are accounted for by including covariates in the scale parameter and assuming a linear change with time:

$$\sigma(t) = \alpha_0 + \alpha_1 t. \quad (3)$$

For the cyclone intensity measures, the time steps have to account for discontinuous occurrence of the life cycle maxima. The method is analogue to generalized linear modelling. Comparing stationary and trend models enables conclusions about trend significance with the test and criteria described below. This method for trend detection in extremes outperforms other methods, like linear least squares estimation or even Kendalls trend test (Zhang, 2004). The main advantage is, that the residuals are not restricted to normal distributed values, which is a wrong assumption in the extreme value context. In the same way, the scale parameter dependance of the NAO time series can be modelled as

$$\sigma(t) = \beta_0 + \beta_1 \text{NAO}(t). \quad (4)$$

Combining eqs (3) and (4) allows to distinguish between the two different impacts. Equivalent, the shape parameter can be modelled with time dependencies as well.

Each of the assumptions increases the number of parameters to be estimated. Instead of σ , one has to estimate α_0 and α_1 to include the linear trend. To avoid overfitting and to test for significant improvement of higher dimensional statistical models log-likelihood ratio tests (LLR-test) are performed (details are given in Coles, 2003). The significance level is set to $\alpha = 0.05$ throughout (LLR-tests and other applied tests). This kind of test is only applicable in the case of nested models, i.e. models with less parameters have to be in subset of models with more parameters. This restriction is overcome by using Akaike's information

criterion (AIC, Akaike, 1974)

$$\text{AIC} = -2 \log[\mathcal{L}(\hat{\theta}|y)] + 2K \left(\frac{n}{n - K - 1} \right) \quad (5)$$

with maximized Likelihood, $\mathcal{L}(\hat{\theta}|y)$, number of estimated parameters, K , and multiplier, $n/(n - K - 1)$. This is a small sample size extension of Akaike's original definition (Burnham and Anderson, 2002). From a set of models with AIC_i (i is the model number), the best model is the one with the minimum AIC value AIC_{\min} . Akaike differences (AICD) are calculated to rank and compare the models

$$\Delta_i = \text{AIC}_i - \text{AIC}_{\min} \quad (6)$$

A guideline for AICD is: $\Delta_i < 2$ gives models with strong, $4 < \Delta_i < 7$ considerably less and $\Delta_i > 10$ no support (Burnham and Anderson, 2002). Further interpretation is achieved with Akaike weights (AICW)

$$w_i = \frac{\exp(-0.5\Delta_i)}{\sum_{j=1}^J \exp(-0.5\Delta_j)} \quad (7)$$

which give the probability that model i is the best one for the given data.

Differences in extremes are commonly analysed in terms of return levels and respective confidence intervals. Additional, extreme value distributions can be compared in terms of their parameters by performing tests for increased or decreased scale or shape parameters. In the following, this is done with the method of time dependant parameters. The data sets of interest (for example ERA40 and 20C) are merged and analysed together. Instead of time t (eq. 3), a step function is included with values of -1 (1) over the time period of the first (second) data set. The scale parameter depends on the selected threshold. To simplify interpretation the higher threshold of the two data sets is applied.

With this concept different statistical models are built, ranging from the 'stationary' model with no difference between the parameters of the two data sets to the model, where both the scale and shape parameter are allowed to change. The different models can then easily be compared and tested employing LLR-test and AIC. With the best model obtained in this way it is possible to reconstruct return level plots for each data set separately. Scale and shape parameters are achieved from the combined model. According to eq. (2) the number of cyclones per year and the exceedance probability are also required which, however, are easily calculated for the corresponding data sets (note: these quantities do not affect model estimation). Confidence intervals can be calculated by resampling.

3. Extreme value statistics and cyclone life cycles

In the following, life cycle maxima of the cyclone intensity measures geopotential height (z_{1000}) mean horizontal gradient (∇z), cyclone depth (D) and relative vorticity (ζ_{850}) are analysed. First, overall density estimates are compared, followed by an investigation of present day extremes and their potential dependance on covariates. The impact of greenhouse gas warming on the extreme statistics concludes this section.

3.1. Density estimates

Before analysing extreme values, estimates for the overall distributions of the variables of interest are evaluated for all data sets (Fig. 1). All estimates show uniform distribution functions. While the central geopotential height, z_{1000} is nearest to a Gaussian distribution, the other quantities are positively skewed (Fig. 1a). The skewness, an important quantity affecting the extremes, is reproduced by ECHAM5/MPI-OM. The deviations

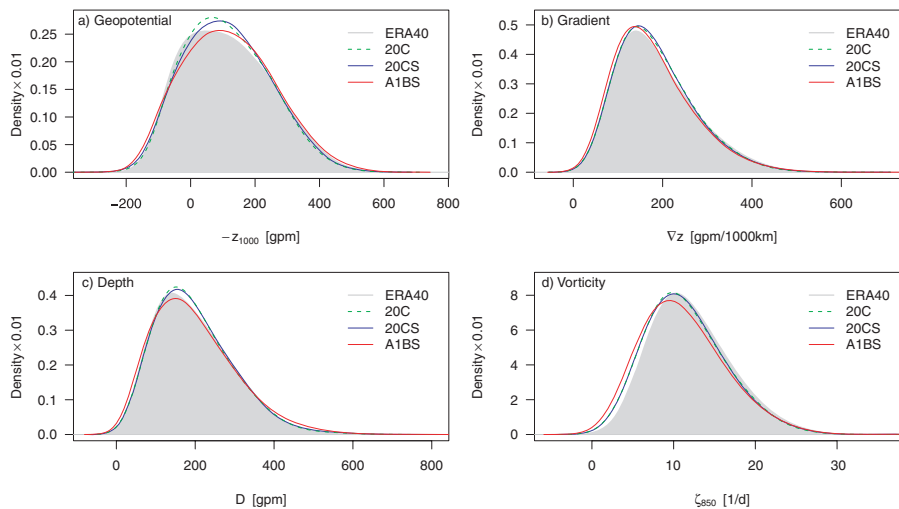


Fig. 1. Kernel density estimates for maximum cyclone life cycle properties of (a) geopotential height, z_{1000} , (b) mean horizontal gradient, ∇z , (c) cyclone depth, D and (d) relative vorticity, ζ_{850} . Used are all data sets in this study, re-analysis (ERA40), transient (20C) and the stabilization model runs (20CS and A1BS).

between observed (ERA40) and model simulated data (20C) are small. The densities agree well, with the exception of the relative vorticity, ζ_{850} where the ECHAM5/MPI-OM density is slightly shifted to lower values (Fig. 1d). Comparing the differences in the mean underlines this. A t -test shows no significant differences between ERA40 and 20C in the z_{1000} , ∇z and D . But the mean ζ_{850} in 20C is significantly lower than in ERA40.

The transient (20C) and stabilization (20CS) model runs give nearly identical results. Despite an assumed higher variability in 20C, probably associated with increasing greenhouse gas forcing, the distributions of the cyclone parameters remain largely unaffected compared to 20CS. This may be an indication of the small importance of the forcing during this (relatively short) time period compared to the natural variability of the system. Larger, but still small differences are visible, if the two stabilization runs 20CS and A1BS are compared. The tail behaviour shows slight differences for z_{1000} and D (Figs. 1a and c). The distributions of ∇z and ζ_{850} are shifted to lower values (Figs. 1b and d). Testing for differences in the mean gives a significant higher z_{1000} in A1BS, no change for D , and significantly reduced values for ∇z and ζ_{850} .

3.2. Extremes of the present day climate

Extreme value statistics is applied to compare the models (20C) present-day climate with observations (ERA40) and to assess the dependence on linear trend and NAO.

3.2.1. Return level estimates. Comparing ERA40 and 20C, Fig. 2 displays return level plots. For return periods below 1 yr the return values are significantly lower in 20C for z_{1000} , ∇z and ζ_{850} . This shift is not present for D .

For the local measures z_{1000} , ∇z and ζ_{850} , the results indicate Weibull-type distributions for both data sets with comparable shapes. The estimated shape parameters, $\hat{\xi}$, together with scales, $\hat{\sigma}$ and thresholds, u are given in Tables 1 and 2. For these two parameters the model exhibits longer return times (lower return levels) compared to the observations. For the integral (large-scale) measure D virtually no difference occur for return periods up to about 10 yr. However, while the shape hints to a Weibull-type distribution for ERA40, a Gumbel-type distribution is plausible for the model ($\hat{\xi} = -0.003$; see Table 2), though this might be caused by sampling errors for long return periods.

To clarify the observed differences in return levels, the GPD are investigated. Return levels are controlled by scale and shape. For z_{1000} the estimated parameters, $\hat{\sigma}$ and $\hat{\xi}$ are similar for 20C and ERA40 (Tables 1 and 2). Larger differences occur for the other quantities, where the scale, the shape or both are affected. One example is the shape parameter for the depth, D , which is consistent with $\xi = 0$ in 20C, but not in ERA40. To decide whether the extreme value distributions are significantly different between the two data sets or, if one distribution could be found that fits the quantities from both data sets equally well combined estimates are calculated (see Section 2). The statistical model set consists of four models: (i) ‘stationary’, no time

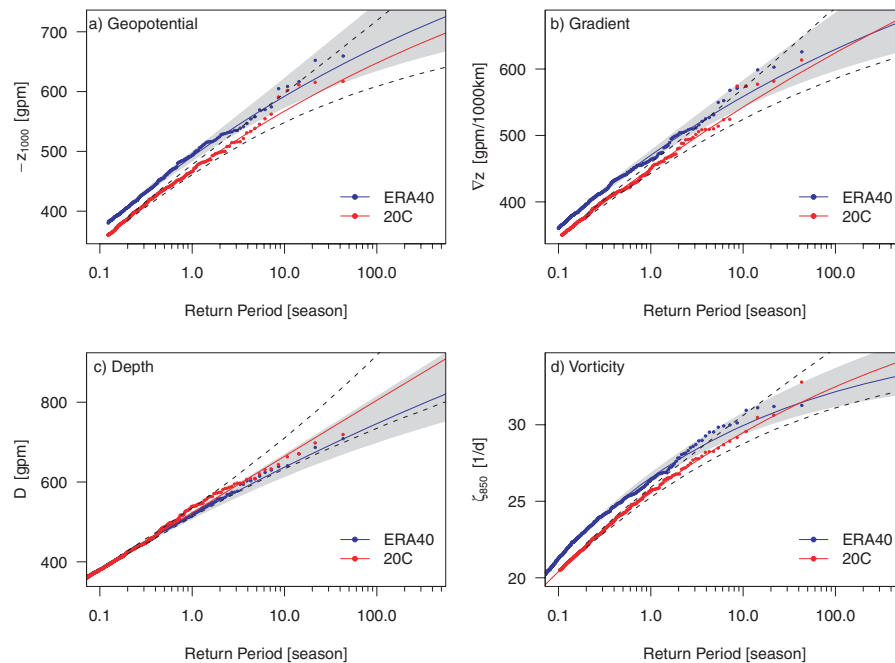


Fig. 2. Return level plots for (a) geopotential height, z_{1000} , (b) mean horizontal gradient, ∇z , (c) cyclon depth, D and (d) relative vorticity, ζ_{850} . The empirical (points) and estimated return levels (lines) have the same colors for ERA40 (blue) and 20C (red). 95% confidence intervals are shown for ERA40 (grey shaded) and 20C (dashed lines).

Table 1. Estimated parameters scale, $\hat{\sigma}$ and shape, $\hat{\xi}$ as well as determined thresholds, u for the selected cyclone properties: geopotential height, z_{1000} , mean horizontal gradient, ∇z , cyclon depth, D and relative vorticity, ζ_{850} for observations (ERA40)

ERA40	u	$\hat{\sigma}$	$\hat{\xi}$	Δ_{stat}	Δ_{trend}	Δ_{NAO}	$\hat{\beta}_1$
z_{1000}	380	58.39 (4.33)	-0.089 (0.052)	6.5 (0.037)	7.7 (0.02)	0.0 (0.943)	7.42 (2.34)
∇z	360	53.31 (3.42)	-0.095 (0.043)	1.7 (0.273)	3.7 (0.099)	0.0 (0.628)	3.9 (1.97)
D	320	64.38 (2.66)	-0.046 (0.029)	0.0 (0.554)	2.0 (0.203)	1.7 (0.243)	1.08 (1.8)
ζ_{850}	20	3.08 (0.16)	-0.191 (0.033)	1.9 (0.255)	3.9 (0.094)	0.0 (0.651)	0.171 (0.085)

Notes: AICD for the ‘stationary’ (Δ_{stat}), linear trend (Δ_{trend}) and NAO model (Δ_{NAO}) are given with AICW in parentheses, as well as estimated slope, $\hat{\beta}_1$ for the NAO model. The standard deviation for estimated parameters is given in parentheses.

Table 2. Like Table 1, but for the transient climate model simulation (20C)

20C	u	$\hat{\sigma}$	$\hat{\xi}$	Δ_{stat}	Δ_{trend}	Δ_{NAO}	$\hat{\beta}_1$
z_{1000}	360	56.8 (4.17)	-0.088 (0.051)	0.0 (0.415)	1.1 (0.243)	0.4 (0.342)	3.435 (2.678)
∇z	350	48 (3.33)	-0.054 (0.048)	0.9 (0.335)	2.6 (0.143)	0.0 (0.522)	3.906 (2.235)
D	350	62.23 (3.51)	-0.003 (0.042)	1.8 (0.251)	2.9 (0.141)	0.0 (0.608)	4.599 (2.308)
ζ_{850}	20.5	2.55 (0.17)	-0.118 (0.045)	0.0 (0.528)	2.0 (0.199)	1.3 (0.273)	0.088 (0.103)

dependance, i.e. the same parameters in ERA40 and 20C, (ii) $\sigma(t)$, (iii) $\xi(t)$ and (vi) $\sigma(t)$ and $\xi(t)$. In (ii)–(iv) the parameters are allowed to be different in ERA40 and 20C.

Applying LLR-test to the statistical models reveals no significant differences in the parameters between ERA40 and 20C for all four cyclone properties (all p -values are higher than 0.15). Furthermore, the AIC minimum is reached with the ‘stationary’ model, with just one exception (not shown). The vorticity reaches the AIC minimum with the $\sigma(t)$ model. However, the ‘stationary’ model is very near to this minimum (with AICD = 0.003) and is preferred due to lower number of parameters. Note that from the combined models reconstructed return levels (not shown) are similar to the curves in Fig. 2. However, the crossing between 20C and ERA40 curves in Fig. 2b (∇z) and Fig. 2d (ζ_{850}) vanishes as an effect of the similar extreme value distributions.

Since, the estimated parameters agree in both data sets, the differences in the return levels result solely from a shift in the location of the distributions. If the thresholds agree, this shift is expressed through differing exceedance probabilities (eq. 2). For ∇z the exceedance probabilities are 0.044 (0.033) in ERA40 (20C). The same argument holds for z_{1000} (ζ_{850}) with probabilities 0.036 (0.067) in ERA40 and 0.026 (0.052) in 20C, respectively. The exceedance probabilities for D reach the same rounded value of 0.073 in ERA40 and 20C. The effect of consistent parameters and exceedance probabilities leads to identical return levels from combined model approach (not shown).

To summarize, GPD with the same scale and shape parameters are found in ERA40 and 20C for each cyclone quantity. Reduced return levels in 20C (z_{1000} , ∇z and ζ_{850}) result from lower

locations of the GPD, which are expressed through smaller exceedance probabilities for agreeing thresholds. A smaller number of threshold crossings may be a direct effect of the lower resolution in 20C, since higher resolution also results in strengthening of cyclones on larger scales as show by Jung (2006) for the ECMWF model.

3.2.2. *Trend and NAO dependance of extremes.* There is evidence, that cyclone properties have changed in the recent past (Ulbrich et al., 2009 and references therein). However, trend analysis using a generalized linear models approach with extreme value distributions has not been undertaken so far. Impacts on the extremes by the covariates, linear trend and NAO, are investigated in ERA40.

LLR-tests applied for the trend model yield p -values higher than 0.3 for each cyclone property. This excludes an influence on the extremes by a linear trend. This is further confirmed by the AICD, where the ranking gives the weakest support for the model with linear trend (Table 1). So that, the trend component (eq. 3) does not improve model fits and the stationary model would be preferred, if this two models are considered.

Using the NAO as covariate (eq. 4) leads to differing findings. For the geopotential height, z_{1000} , the applied LLR-test gives high significance for the NAO outperforming the stationary model (p -value lower than 0.005). The LLR-test is passed too, if the vorticity, ζ_{850} , is considered. The depth, D , fails the test. The p -value for the gradient, ∇z , is just slightly higher than the chosen α (p -value = 0.054). The AIC best model is achieved with the NAO as a covariate with ∇z , as for z_{1000} and ζ_{850} . Furthermore the estimated $\hat{\beta}_1$ is high enough to exclude $\beta_1 = 0$ compared to the given range by the standard deviation. Giving weight to the conclusion that the NAO improves model fits also for ∇z .

However, the strength of support is lower as for z_{1000} and reaches nearly the same probability as ζ_{850} .

The observed NAO exhibits decadal-like trends, being upward directed from the sixties until the end of the eighties. This together with an assumed increase in the cyclone quantities through greenhouse gas warming might be interpreted as the NAO just reflecting this upward trend. This possibility however, could be excluded through the given trend analysis, stating no significant trend.

In summary, strong support is found that the NAO has an impact on the geopotential height, z_{1000} , extremes. The same holds also for ∇z and ζ_{850} , but with restrictions on the strength of evidence. This is consistent with results found by Pinto et al. (2009), that is, higher cyclone intensities ($\nabla^2 p$) and deeper cores are related to the daily projected positive NAO phases. Here we extend this finding to the gradient, ∇z . Furthermore covariate modelling with the monthly NAO leads to the probabilistic interpretation that, in months with positive (negative) NAO, the probability of extreme intense cyclones is increased (decreased).

In agreement with ERA40 no significant trend could be found in 20C in none of the cyclones quantities (p -values higher than 0.3). With AIC decision making is hampered because all AICD are smaller than 3, demonstrating plausibility for each model. But the trend model gives highest AICD and the estimated slope, $\hat{\alpha}_1$, is smaller than the corresponding standard deviation (not shown). Therefore, the trend exclusion with AIC is not as strong as in ERA40.

With the NAO-model an improvement is only present for depth, D , with an achieved p -value near the significance level (p -value: 0.052). Most striking is the strongly reduced evidence of the NAO impact on z_{1000} extremes in 20C, which is clearly present in ERA40 (see AICW values in Table 2). The small AICD however, indicates an improvement of the model fit, confirmed by $\hat{\beta}_1$ with smaller standard deviation than parameter estimate. But the improvement is too weak to separate it from the stationary model on the basis of AICD alone.

Further differences are found for the NAO influence on D and ζ_{850} extremes: AICD gives weak support for D in 20C

(probability around 60%), which is not present in ERA40. The weak support for ζ_{850} in ERA40 is vanished in 20C showed by the parameter estimate, $\hat{\beta}_1$, including 0 if referred to the standard deviation. The dependance of ∇z on the NAO is the same in ERA40 and 20C, with slightly reduced probability.

To summarize, the differences between observed (ERA40) and modelled (20C) cyclone dependencies consist mainly in the strength of support for the statistical models chosen. Differing findings may not necessarily result from a dynamic response missing in the model. Another possibility is the time evolution of the observed NAO in the ERA40 period, which exhibits decadal trends. A phase shift of these trends in the model could be an explanation. Note that the overall agreement with ERA40 is higher in 20CS (see below) reflecting a strong sensitivity to the sampling size (which is, of course, also true for ERA40).

3.2.3. *Excursion, NAO and z_{1000} extremes in ERA40.* The impact of the NAO on the z_{1000} return levels is illustrated in Fig. 3a. The lines correspond to ‘NAO-worlds’, i.e. the NAO is held fixed on the selected levels from -2 to 2 and are calculated with the determined parameters from the covariate model. Using eq. (4) with estimated $\hat{\beta}_1$ from Table 1 results in a scale parameter difference of almost 30 gpm between $NAO = -2$ and $NAO = 2$. This difference has a large impact on the calculated return levels. The return level which is exceeded once every 100 yr with $NAO = -2$ is roughly 570 gpm (lower horizontal grey line). The return period is largely reduced with $NAO = 2$, the same level is now exceeded every 3–4 yr or, on the other hand, the 100 yr return level is increased up to more than 700 gpm (upper horizontal grey line).

Note that the stationary model (grey line in Fig. 3a) gives similar results as $NAO = 1$ and not, as one might expect the neutral $NAO = 0$ case. The reason for this departure is the disproportional occurrence of threshold exceedances, as there are 73.9% (26.1%) threshold crossings in the positive (negative) NAO phase. This difference in number affects the maximization procedure, which is dominated by the majority of values.

Figure 3b confirms the results with another method. Here, compositing extremes is applied to achieve GPD for the case where the NAO is greater (less) than 0.5 (-0.5). The grey line

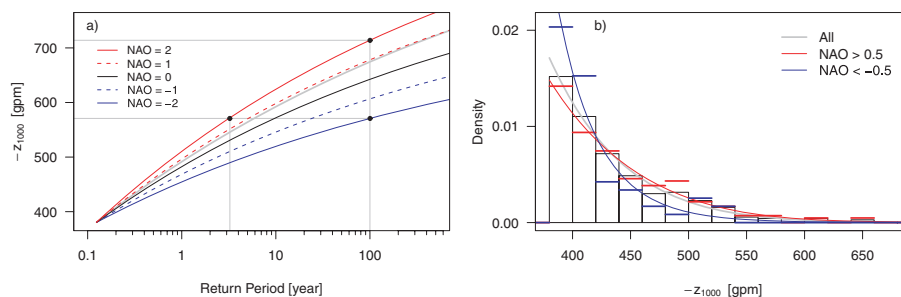


Fig. 3. NAO impact on geopotential height, z_{1000} extremes. (a) Return levels for given NAO value from -2 to 2 , influencing the GPD scale parameter. (b) Histograms, as well as estimated density for GPD, for composites of z_{1000} extremes, where NAO exceeding (falling below) 0.5 (-0.5) and all values together.

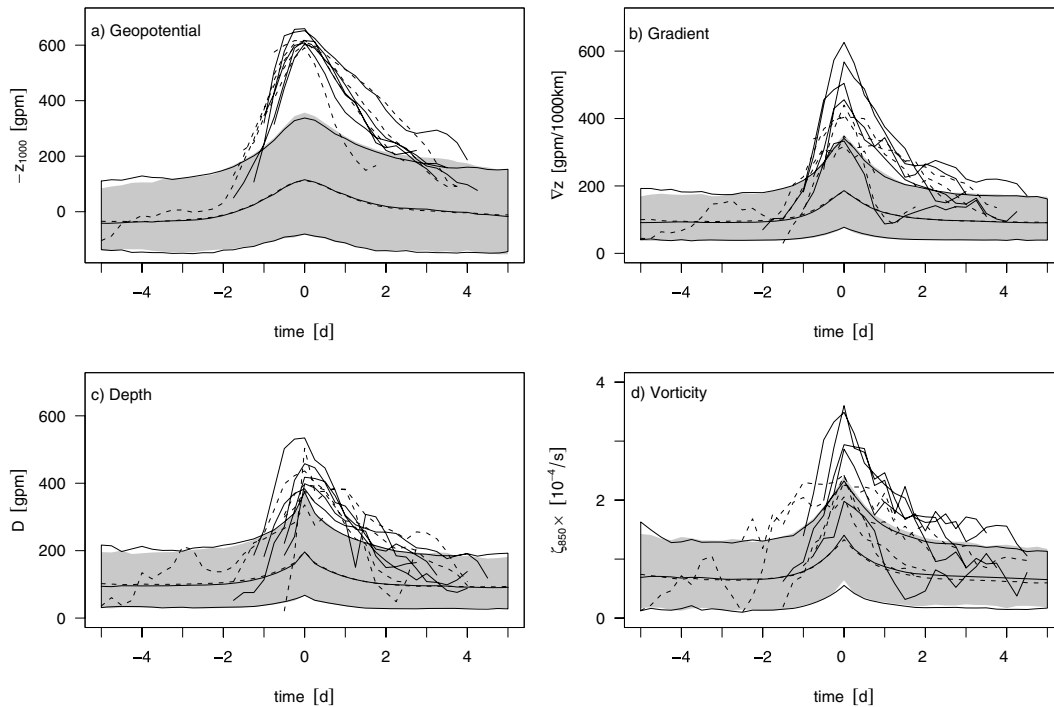


Fig. 4. The five most extreme life cycles in respect of z_{1000} centred about the extremum for (a) geopotential height, z_{1000} , (b) mean horizontal gradient, ∇z , (c) cyclone depth, D and (d) relative vorticity, ζ_{850} for ERA40 (solid) and 20C (dashed). Ninety percent of the data (confined by the 5 and the 95 quantile) are presented by shaded (framed) region for ERA40 (20C).

gives the resulting distribution of the stationary fit (using all values above the threshold). The estimated distributions agree well with the corresponding histograms. The impact of the NAO on the extremes gives higher (lower) densities for $\text{NAO} < -0.5$ ($\text{NAO} > 0.5$) for small values. This relation is reversed for values exceeding ≈ 425 gpm. The deviations of the $\text{NAO} > 0.5$ ($\text{NAO} < -0.5$) distributions, compared to the fit with all values, are small (large).

3.2.4. Life cycles and spatial occurrence of extremes. The mean life cycles of the four cyclone parameters are shown in Fig. 4 for all cyclones in ERA40 and 20C, as well as the 95 and 5% quantiles. Additionally, the individual life cycles of the five most extreme cyclones are included, whereas extreme is related to z_{1000} . For all parameters, the mean life cycles are in good agreement between ERA40 and 20C. If the life cycles of the five most extreme cyclones in the respective parameter are considered, the good agreement is confirmed (not shown). An extreme cyclone in z_{1000} may not naturally belong to an extreme cyclone in the other variables. However, nearly all extreme cyclones with respect to z_{1000} belong to the most extreme upper 5% in the other variables for ERA40. The same holds if another reference parameter is chosen. Similar results but with reduced absolute values in terms of z_{1000} occur in 20C.

The spatial density estimates of the locations where the life cycle maxima occur are shown in Fig. 5 for the selected quan-

ties geopotential height, z_{1000} and the relative vorticity, ζ_{850} . Only cyclones are included whose maxima pass the according threshold (see Tables 1 and 2). Comparing the density maxima of z_{1000} and ζ_{850} for ERA40 (Figs. 5a and c, respectively) yield two different positions of the centres. The spatial density estimates with respect to the gradient (not shown) indicate a maximum in between the maxima of ζ_{850} and z_{1000} . Note that, the spatial density estimates consider the maxima of extreme cyclones in the accordant parameter only. Therefore, the number of the considered cyclones varies.

For example, a spatial large cyclone with very deep core pressure does not necessarily exhibit a strong wind field and high vorticity values. This circumstance could be responsible for the different cyclone extreme behaviour. Considering only cyclones belonging to the intersection of extreme events in both cyclone variables, z_{1000} and ζ_{850} , the spatial density maxima of z_{1000} is shifted to lower latitudes (not shown) overlapping with the maxima in ζ_{850} . The determined cross correlation function (not shown) of the extreme cyclone life cycles suggest to a time shift (roughly 6 hours) between the vorticity and central geopotential height. This is consistent with Bengtsson et al. (2009) showing that vorticity reaches the maximum before surface pressure. From the geostrophic adjustment it would follow that the mass field leads the wind field if the considered scale is greater than the Rossby radius of deformation. Note that our results indicate the opposite case.

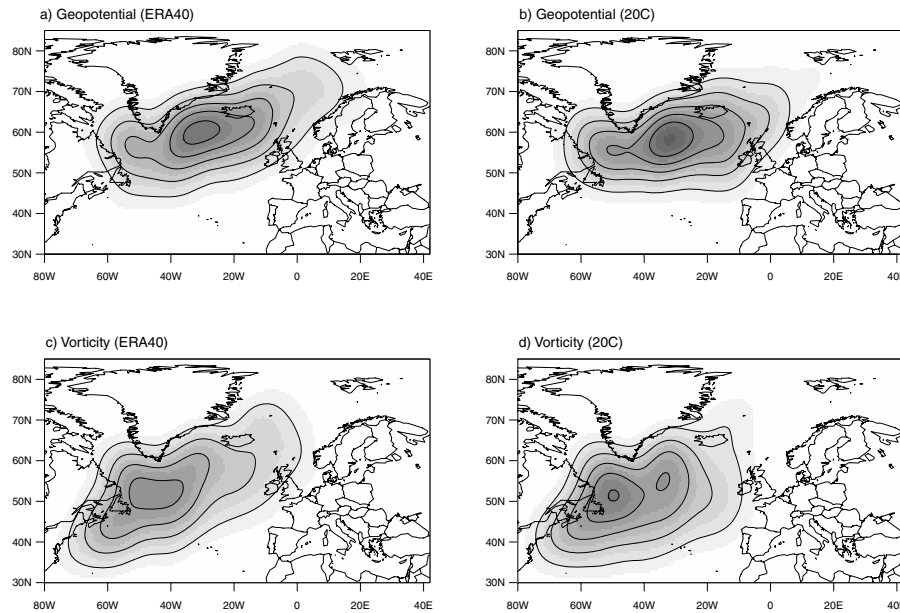


Fig. 5. Spatial density estimates of the most extreme cyclones (values above thresholds) in the centred geopotential height, z_{1000} (upper panels) and the relative vorticity, ζ_{850} (lower panels) for ERA40 (left) and 20C (right).

In 20C, the spatial density estimates of the four parameters correspond to the densities of ERA40. Due to a coarser resolution the spatial variability is smaller in the simulation.

3.3. Extremes changing with greenhouse warming

The stabilization model runs 20CS (present-day) and A1BS (greenhouse warming scenario) are investigated for changing cyclone extremes.

3.3.1. Return level estimates. Changes of the return periods (levels) are displayed in Fig. 6 comparing 20CS and A1BS. For a better comparison, the stabilization run 20CS is used instead of the transient run 20C. It should be noted that a comparison between 20C and 20CS yields differences in the estimated parameters (Table 2 and 3). For all four cyclone properties a higher scale and lower shape parameter is found in 20CS. The 20CS return level curves, however, are located inside the 20C confidence bounds over the full range of return periods (not shown). An explanation for the differences is the smaller sample size in 20C, resulting in large variability from sample to sample, together with sensitive shape parameter estimation and compensating effects between the two parameters.

The return levels show qualitatively consistent results for all variables which, however, vary in detail. In the A1BS climate, a significant shift towards higher return levels (shorter periods) is only found for z_{1000} up to return periods of about 10 yr. The tendency to stronger cyclones is still present but less notable for ∇z and ζ_{850} . For D a consistent shift can be seen for longer (>6 yr) and shorter (<1 yr) periods while medium periods show only a very weak signal. Remarkable is the change from Weibull to Gumble type distribution, indicated by the approximate straight return level curve for D in A1BS. This is con-

firmed through the estimated shape parameter, where $\xi = 0$ is included in the interval given by the standard deviation. However, changes in terms of return levels are not significant for ∇z , ζ_{850} and D .

Deeper insight into the observed return level changes can be achieved by analysing the GPD parameters. In 20CS and A1BS similar shape parameters are found for z_{1000} , ∇z and ζ_{850} (Tables 3 and 4), while the scale parameters are increased in A1BS. Different behaviour is found for depth, D with lower scale and higher shape parameter in A1BS. Combined estimates are calculated and LLR-tests are applied in two steps: first, $\sigma(t)$ - and $\xi(t)$ -models are compared to the ‘stationary’ model (LRT-test 1) and second, the model allowing for different σ and ξ parameters in the data sets is compared to all lower dimensional models (LRT-test 2). For z_{1000} , ∇z and ζ_{850} the ‘stationary’ model with the same parameters in 20CS and A1BS is implausible (Table 5); LLR-test1 favours the $\sigma(t)$ -model against the stationary model since the p -values are all lower than 0.01. Also, the $\xi(t)$ -model shows an improvement, but the reason for this seems to be a compensating effect. This is demonstrated by LLR-test2, because the combined model (σ and ξ are allowed to change; Table 5) outperforms the $\xi(t)$ -, but not the $\sigma(t)$ -model, demonstrating that a change in the scale is sufficient to describe the changes that occur in A1BS. Accordingly the AIC minimum is achieved by the $\sigma(t)$ -model with AICW above 0.5. Interestingly, for ζ_{850} extremes, where the smallest differences in the return levels are obtained, the highest confidence is found for different scale parameters (AICW; $w_{\zeta} = 0.726$). For D , a single time dependant model does not give an improvement compared to the ‘stationary’ model, but allowing for changes in both parameters outperforms all other models.

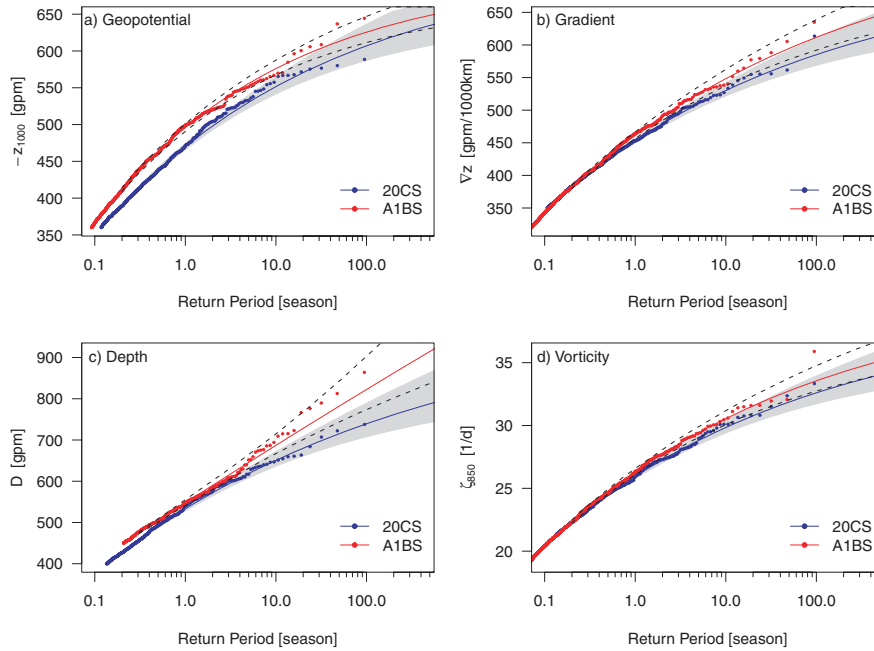


Fig. 6. Like Fig. 2, for the 21th (22th) stabilization run 20CS (A1BS).

Table 3. Like Table 1, for the 21th-century stabilization run (20CS)

20CS	u	$\hat{\sigma}$	$\hat{\xi}$	Δ_{stat}	Δ_{NAO}	$\hat{\beta}_1$
z_{1000}	360	61.37 (2.98)	-0.169 (0.034)	17.1 (0)	0 (1)	7.32 (1.543)
∇z	350	54.33 (2.37)	-0.146 (0.028)	5.2 (0.068)	0 (0.932)	4.19 (1.509)
D	400	75.31 (4)	-0.124 (0.038)	0 (0.687)	1.6 (0.313)	1.771 (2.674)
ζ_{850}	21	2.75 (0.13)	-0.151 (0.031)	0 (0.712)	1.8 (0.288)	0.034 (0.076)

Table 4. Like Table 1 for the 22th-century stabilization run (A1BS)

A1BS	u	$\hat{\sigma}$	$\hat{\xi}$	Δ_{stat}	Δ_{NAO}	$\hat{\beta}_1$
z_{1000}	360	72.43 (2.8)	-0.21 (0.024)	3.9 (0.122)	0 (0.878)	4.497 (1.737)
∇z	300	66.27 (2.04)	-0.138 (0.02)	0 (0.664)	1.4 (0.336)	1.091 (1.356)
D	450	62.75 (4.04)	-0.013 (0.044)	0 (0.712)	1.8 (0.288)	1.26 (2.71)
ζ_{850}	19	3.26 (0.11)	-0.149 (0.02)	0.5 (0.438)	0 (0.562)	-0.111 (0.071)

Table 5. Statistical model building to test for differences between 20CS and A1BS. Estimated p -values according to log-likelihood ratio tests (LLR-test)

20CS-A1BS	LLR-test 1		LLR-test 2			AICD (AICW)			
	$\sigma(t)$	$\xi(t)$	Stat.	$\sigma(t)$	$\xi(t)$	Stat.	$\sigma(t)$	$\xi(t)$	$\sigma(t); \xi(t)$
z_{1000}	0.002	0.057	0.001	0.329	0.008	7.7 (0.013)	0 (0.603)	6.1 (0.028)	1.1 (0.356)
∇z	0.006	0.025	0.006	0.78	0.114	5.4 (0.038)	0 (0.573)	2.4 (0.171)	1.9 (0.218)
D	0.259	0.635	0.025	0.053	0.029	1 (0.268)	1.7 (0.185)	2.8 (0.11)	0 (0.437)
ζ_{850}	0	0.001	0	0.966	0.003	18.6 (0)	0 (0.726)	9 (0.008)	2 (0.266)

Notes: LLR-test1 tests for significant improvement of the time dependant models [$\sigma(t)$ or $\xi(t)$] against the ‘stationary’ model, while LLR-test2 tests the combined model ($\sigma(t)$ and $\xi(t)$ are time dependant) against the lower dimensional models [‘stationary’, $\sigma(t)$ or $\xi(t)$]. Further, AIC differences (AICD) are given with corresponding AIC weights (AICW) in parentheses for all models in the set.

3.3.2. *NAO dependance of extremes.* For both runs (20CS and A1BS) strong support is found for a link to the NAO for z_{1000} , but with reduced strength in A1BS (β_1 reaches 7.3 gpm in 20CS, but only 4.5 gpm in A1BS). That is, other parameters controlling z_{1000} are more important in A1BS than in 20CS. The results may suggest that the increased return levels in A1BS do not result from changed NAO regimes.

For D both data sets do not support a link. Differences are found for ∇z and ζ_{850} : While for ∇z a link is supported in 20CS only, the opposite is true for ζ_{850} . Note that the results for 20CS and 20C differ with respect to the NAO link, which is most probably due to the different sample size.

In contrast to the trend analysis (Section 3.1), differences are found between 20CS and A1BS cyclone extremes, indicating that a linear trend should be present in 20C. The trend on the chosen ERA40 time period, however, is too small to be detectable. Trend detection is further hampered through the presence of NAO, which increases the variability, but this problem is minimized through the method of statistical model building, which is able to separate different impacts on the extremes.

3.3.3. *Lifecycles and spatial occurrence of extremes.* Similar to Fig. 4, the five most extreme life cycles with respect to z_{1000} in the four parameters and the mean life cycles are shown in Fig. 7 for 20CS and A1BS. If the mean life cycles in z_{1000} are considered, a deepening of the cyclones is found in A1BS. Additionally, the variability in z_{1000} increases. The five most extreme life cycles corroborate this finding by showing a decrease in the central geopotential height (higher z_{1000} values). Considering the

mean life cycles in the gradient, ∇z , the relative vorticity, ζ_{850} , and the depth, D , yields opposite conclusions. While the maxima in the gradient and the vorticity decrease, the maxima in the depth are unchanged. Note that the life cycles with respect to z_{1000} in ∇z , ζ_{850} and D belong to the upper 5% of the cyclones.

Indicated by Fig. 6 the extreme cyclones intensify in the warmer climate. Ensuring that this strengthening is not a consequence of a northward displacement of the cyclone tracks, spatial density estimates of the extreme cyclones are compared in Fig. 8. The comparison between the density maxima in the geopotential height reveal no appreciable northward shift of the extreme cyclones between 20CS and A1BS. This is confirmed by spatial density differences yielding no systematic, but rather small and noisy departures (not shown). The density estimates of the other three parameters (ζ_{850} , ∇z and D) indicate a slight increase of the affected area with no northward displacement in connection with a smaller density maximum. Therefore, the intensification of the extreme cyclones found in a warmer climate scenario is supported.

4. Summary, conclusion and discussion

Extreme value statistics is applied to extremes of four parameters characterizing cyclone life cycles: central geopotential height (z_{1000}), mean geopotential height gradient (∇z), cyclone depth (D) and relative vorticity (ζ_{850}). The present-day climate of the coupled atmosphere ocean model ECHAM5/MPI-OM is compared with ERA40 re-analysis and with a global warming

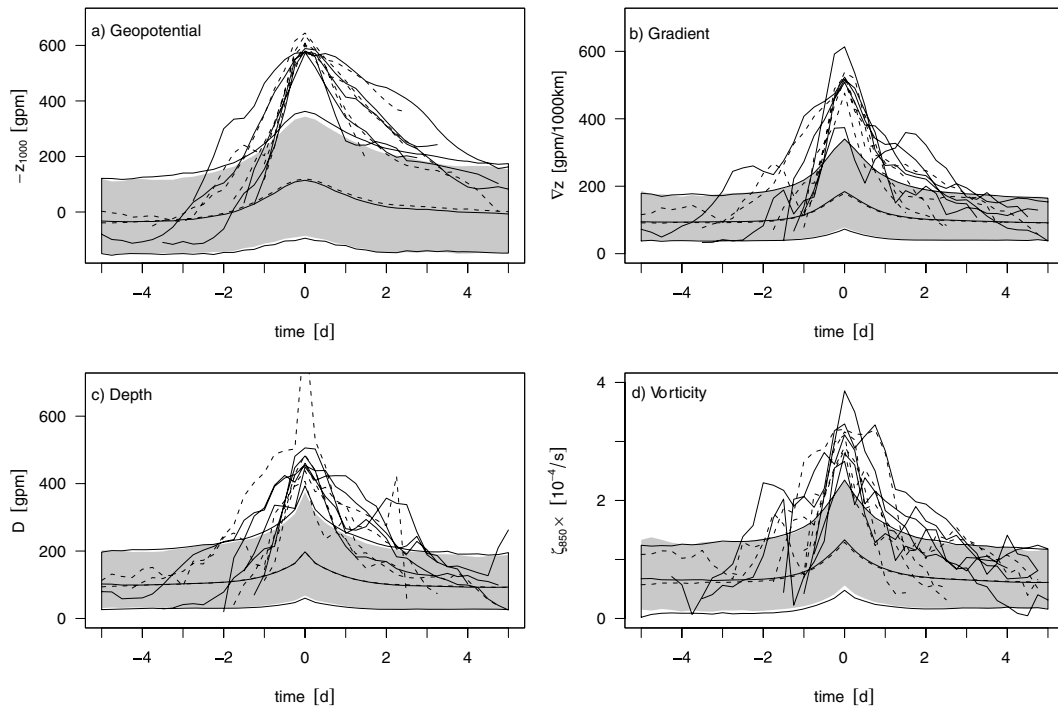


Fig. 7. Like Fig. 4, for the stabilization runs 20CS (solid) and A1BS (dashed).

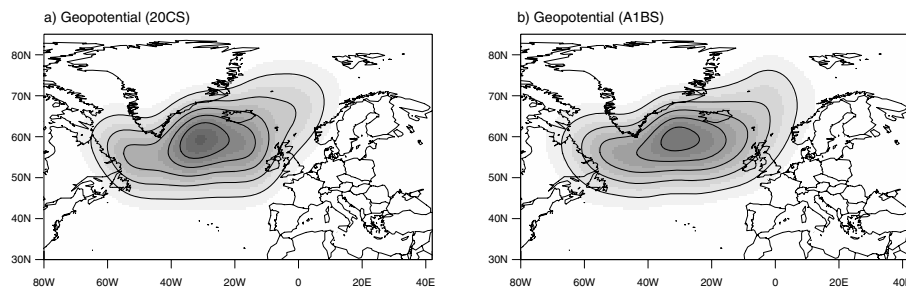


Fig. 8. Spatial density estimates of the most extreme cyclones (values above thresholds) in the centred geopotential height, z_{1000} for 20CS (left) and A1BS (right).

scenario (A1BS). The study focuses on extreme mid-latitude cyclones in the North Atlantic during extended boreal winters (October-March). Additionally, the present-day data (ERA40, 20C) is analysed with respect to a possible trend and a potential link to the NAO is investigated.

In general, the model results are similar in terms of distributions, trends, life cycles and density estimates compared to ERA40. The extreme value statistics (return level plots) for z_{1000} , ∇z and ζ_{850} indicate reversed Weibull-type distributions, implying an upper bound. When analysing the relatively short ERA40 time period, no significant linear trend is detected for ERA40 and 20C simulation. The use of a linear trend model is questionable under the assumption of a non-linear forcing, but higher order polynomial or exponential trends can be approximated through linear models on short time spans. Life cycles of extreme cyclones respective to one cyclone parameter show that these cyclones also belong to the upper tails of the distributions in the other parameters for both, ERA40 and 20C. Density estimates of extreme cyclones in the four cyclone variables of 20C show similar spatial distributions as ERA40. For both data sets, the maximum density in vorticity is located more south than the maxima of the geopotential height.

Apart from these similarities, some differences between the data sets can be noted: The depth, D , shows a Gumbel-type distribution for 20C, while a Weibull-type is obtained for ERA40. In addition, 20C shows lower return levels. The threshold is rarely exceeded, which might be a direct consequence of the lower resolution. In 20C the link between NAO and z_{1000} is less evident than in ERA40. However, much stronger evidence is found in 20CS which may indicate that 40 yr of data are not enough to give robust results.

The comparison between the two stabilization runs (20CS, A1BS) using extreme value statistics yields an intensification of the extreme cyclones in the North Atlantic region. The return levels show an increase for all parameters under consideration, but different in strength: smaller changes for gradient and vorticity and stronger for geopotential and depth. This intensification results in increased scale parameters for z_{1000} , ∇z and ζ_{850} . Additionally, the exceedance probability increases for z_{1000} . For D a decreased scale and increased shape parameter is found. Further

analysis indicates that the deepening in z_{1000} is not a consequence of a northward shift, but could be attributed to changes in the mean sea level pressure (Fink et al., 2009).

Comparing this results with the findings of Della-Marta and Pinto (2009), some differences can be identified. In contrast to their work z_{1000} return values increase for return periods up to 10 yr. However, the results of the vorticity agree. The difference could be attributed to the distinct analysed time period (transient instead of stabilization model run) or the applied tracking algorithm. An extension is the analysis of GPD parameters. With the exception of D , each cyclone quantity (z_{1000} , ∇z and ζ_{850}) shows a higher scale parameter in A1BS. Demonstrating that significant different parameters do not necessarily yield a significant difference in return values.

Extreme cyclones and their trends have been analysed in both model simulations and observations (re-analyses). However, a comparison with the results presented here is hampered by (i) different cyclone identification and tracking, (ii) different definitions of cyclone extremes and intensity measures and (iii) different methodology to assess their statistics. Although for the entire Hemisphere, Ulbrich et al. (2009) already noted that dependant on the definition of extreme cyclones both an increase and a decrease in extreme cyclones can be found for the Northern Hemisphere: analysing extreme cyclones in the upper percentage of extremely low sea level pressure they detect an increase of extreme cyclones in a A1B greenhouse warming scenario, while the definition of extremes by high values in the pressures Laplacian yields a decrease.

Despite the limited comparability the following similarities and differences with regard to recent studies might be noted: A link to NAO is confirmed by Pinto et al. (2009) showing that the number of extreme cyclones is enhanced in positive NAO phase in the NCEP/NCAR re-analyses. The absence of a significant trend in the cyclone parameters for the whole North Atlantic is consistent with the findings of Raible et al. (2008) (using NCEP/NCAR and ERA40 re-analyses). But, dividing the North Atlantic region in a high latitude and a mid-latitude part, similar to the defined regions of Wang et al. (2008), Raible et al. (2008) find a dipole-like trend pattern in cyclone activity (in agreement with Wang et al., 2008) and intensity.

Based on a multimodel perspective, there is a reduction in the total number of cyclones on the hemisphere in warmer climate simulations, whereas an increase is found in intense systems (Lambert and Fyfe, 2006). The decrease of the total number of cyclones in the Northern Hemisphere is supported by several other studies (Bengtsson et al., 2006; Finnis et al., 2007; Löptien et al., 2008; Pinto et al., 2009). Comparing 20th century to warmer climate simulations, a northward shift of all detected cyclones is found. Cyclone density increases near the British Isles during the transient A1B scenario, while this increase is absent in the stabilization runs (not shown).

Consistent with the results presented here, Löptien et al. (2008) observe stronger deepening rates. However, they do not find significant changes in cyclone intensity (minimum central pressure during the cyclone life cycle). Deeper central core pressures of the 100 most intense cyclones were found in scenario A1B, but interpreted as a result of a northward shift of cyclone tracks (Bengtsson et al., 2009).

An increased track density and intensity of extratropical cyclones is found near the British Isles in warmer climate scenarios (Ulbrich et al., 2009 and references therein). The same holds for extreme cyclones (Pinto et al., 2009) and is detected in multimodel analysis (Leckebusch et al., 2006).

Evaluating the present study concerning a possible change it is interesting to note that if all detected cyclones are used a strengthening can only be found for z_{1000} . The other parameters would indicate no change (D) or a weakening ($\nabla z, \zeta_{850}$). This demonstrates potential advantages of analysing the extremes directly. As presented here, extreme value statistics appears to be an appropriate and powerful method. In addition, accounting every cyclone only once to avoid intense and long living cyclones to be disproportionately weighted and to ensure independent data is preferable.

To supplement this study it may be useful to analyse and compare cyclones detected from the vorticity field and to ascertain the causes of the different positions of the density maxima found for the different cyclone parameters. Regarding the cyclone variable D , one can only speculate why D differs in general for the other results. Here, further analyses are needed, for example, regarding the sensitivity to the particular definition of D .

Furthermore, possible links between North Atlantic cyclone extremes and variability modes other than NAO may be detectable (for example, El Niño/Southern Oscillation (ENSO) or the stratospheric circulation). Since it is possible to identify a significant change of extreme cyclones analysing the A1BS stabilization run, but not within the ERA40 period, the question arises how sufficiently large the sample size should be for trend identification.

Considering the North Atlantic basin the determining factors for a cyclone to belong to an extreme event changes in A1B. Due to an enhanced low-level temperature gradient in the central North Atlantic, the low-level baroclinicity increase (Bengtsson et al., 2006). This region is also characterize by an eastward

shift of the polar jet stream into Europe and increased upper air baroclinity (Pinto et al., 2007), which are related to extreme cyclones.

The present work can be integrated in the context of statistical analysis of cyclone extremes in re-analysis, present-day and future scenarios. Understanding the physical mechanisms behind the changes on cyclone extremes and the different behaviour of cyclone variables on NAO are part of further analysis.

5. Acknowledgments

We like to thank two anonymous reviewers for their helpful comments and suggestions. Thanks to Ulrike Port for help on the analysis. The R Development Core Team (2009) is acknowledged for providing the statistics package ‘R’. This work has been supported by Deutsche Forschungsgemeinschaft (SFB-512).

References

- Akaike, H. 1974. A new look at the statistical model identification. *IEEE Trans. Automat. Contr.* **19**, 716–723.
- Benedict, J. J., Lee, S. and Feldstein, S. B. 2004. Synoptic view of the North Atlantic Oscillation *J. Atmos. Sci.* **61**, 121–144.
- Bengtsson, L., Hodges, K. I. and Roeckner, E. 2006. Storm tracks and climate change *J. Clim.* **19**, 3518–3543.
- Bengtsson, L., Hodges, K. I. and Keenlyside, N. 2009. Will extratropical storms intensify in a warmer climate? *J. Clim.* **22**, 2276–2301.
- Blender, R., Fraedrich, K. and Lunkeit, F. 1997. Identification of cyclone-track regimes in the North Atlantic. *Q. J. R. Meteorol. Soc.* **123**, 727–741.
- Burnham, K. P. and Anderson, D. R. 2002. *Model Selection and Multimodel Inference: A Practical Information-Theoretical Approach*, Springer-Verlag, New York. 496pp.
- Coles, S. 2003. *An Introduction to Statistical Modeling of Extreme Values*, Springer-Verlag, London. 224pp.
- Della-Marta, P. M. and Pinto, J. G. 2009. Statistical uncertainty of changes in winter storms over the North Atlantic in an ensemble of transient climate simulations. *Geophys. Res. Lett.* **36**, L14703.
- Fink, A. H., Brücher, T., Ermert, V., Krüger, A. and Pinto, J. G. 2009. The European storm Kyrill in January 2007: synoptic evolution, meteorological impacts and some considerations with respect to climate change. *Nat. Hazards Earth Syst. Sci.* **9**, 405–423.
- Finnis, J., Holland, M.M., Serreze, M. C. and Cassano, J. J. 2007. Response of northern hemisphere extratropical cyclone activity and associated precipitation to climate change, as presented by the community climate system model. *J. Geophys. Res.* **112**, G04S42.
- Gulev, S. K., Zolina, O. and Grigoriov, S. 2001. Extratropical cyclone variability in the Northern Hemisphere winter from the NCEP/NCAR reanalysis data. *Clim. Dyn.* **17**, 795–809.
- Hodges, K. I. 1994. A general method for tracking analysis and its application to meteorological data. *Mon. Wea. Rev.* **122**, 2573–2586.
- Jung, T., Gulev, S. K., Rudeva, I. and Soloviov, V. 2006. Sensitivity of extratropical cyclone characteristics to horizontal resolution in the ECMWF model. *Q. J. R. Meteorol. Soc.* **132**, 1839–1858.

- Jungclaus, J. H., Keenlyside, N., Botzet, M., Kaak, H., Luo, J.-J. and co-authors. 2006. Ocean circulation and tropical variability in the coupled model ECHAM5/MPI-OM. *J. Clim.* **19**, 3952–3972.
- Katz, R. W., Parlange, M. B. and Naveau, P. 2002. Statistics of extremes in hydrology. *Adv. Water Resour.* **25**, 1287–1304.
- Kharin, V. V. and Zwiers, F. W. 2000. Changes in the extremes in an ensemble of transient climate simulations with a coupled atmosphere-ocean GCM. *J. Clim.* **13**, 3760–3788.
- Kharin, V. V. and Zwiers, F. W. 2005. Estimating extremes in transient climate simulations. *J. Clim.* **18**, 1156–1173.
- Lambert, S. J. and Fyfe, J. C. 2006. Changes in winter cyclone frequencies and strengths simulated in enhanced greenhouse warming experiments: results from the model participating in the IPCC diagnostic exercise. *Clim. Dyn.* **26**, 713–728.
- Leckebusch, G. C., Koffi, B., Ulbrich, U., Pinto, J. G., Spanghel, T. and co-authors. 2006. Analysis of frequency and intensity of European winter storm events from a multi-model perspective, at synoptic and regional scales. *Clim. Res.* **31**, 59–74.
- Löptien, U. and Ruprecht, E. 2005. Effect of synoptic systems on the variability of the North Atlantic Oscillation. *Mon. Wea. Rev.* **133**, 2894–2904.
- Löptien, U., Zolina, O., Gulev, S., Latif, M. and Soloviev, V. 2008. Cyclone life cycle characteristics over the Northern Hemisphere in coupled GCMs. *Clim. Dyn.* **31**, 507–532.
- Mailier, P. J., Stephenson, D. B., Ferro, C. A. T. and Hodges, K. I. 2006. Serial clustering of extratropical cyclones. *Mon. Weather Rev.* **134**, 2224–2240.
- Marsland, S. J., Haak, H., Jungclaus, J. H., Latif, M. and Röske, F. 2003. The Max-Planck-Institute global ocean/sea ice model with orthogonal curvilinear coordinates. *Ocean Model.* **5**, 91–127.
- Murray, R. J. and Simmonds, I. 1991. A numerical scheme for tracking cyclone centers from digital data. Part I: development and operation of the scheme. *Aust. Meteor. Mag.* **39**, 155–166.
- Nakicenovic, N., Alcamo, J., Davis, G., de Vries, B., Fenhann, J. and co-authors. 2000. *Special Report on Emissions Scenarios*, (eds N. Nakicenovic and R. Swart), Cambridge University Press., Cambridge, 599pp.
- Pinto, J. G., Ulbrich, U., Leckebusch, G. C., Spanghel, T., Reyers, M. and co-authors. 2007. Changes in storm track and cyclone activity in three SRES ensemble experiments with the ECHAM5/MPI-OM1 GCM. *Clim. Dyn.* **29**, 195–210.
- Pinto, J. G., Zacharias, S., Fink, A. H., Leckebusch, G. C. and Ulbrich, U. 2009. Factors contributing to the development of extreme North Atlantic cyclones and their relationship with the NAO. *Clim. Dyn.* **32**, 711–737.
- R Development Core Team 2009. R: A language and environment for statistical computing. R Foundation for Statistical Computing, Vienna, Austria. <http://www.R-project.org>.
- Raible, C. C., Della-Marta, P. M., Schwierz, C., Wernli, H. and Blender, R. 2008. Northern Hemisphere extratropical cyclones: a comparison of detection and tracking methods and different reanalyses. *Mon. Wea. Rev.* **136**, 880–897.
- Roeckner, E., Bäuml, G., Bonaventura, L., Brokopf, R., Esch, M. and co-authors. 2003. The atmospheric general circulation model ECHAM5. Part I: model description. *MPI Rep.* **349**, 127pp.
- Schneider, A., Blender, R. and Fraedrich, K. 2010. Radius-depth model for midlatitude cyclones in re-analysis Data and Simulations. *Q. J. R. Meteor. Soc.* **136**, 50–60.
- Sickmüller, M., Blender, R. and Fraedrich, K. 2000. Observed winter cyclone tracks in the Northern Hemisphere in re-analysed ECMWF data. *Q. J. R. Meteor. Soc.* **126**, 591–620.
- Ulbrich, U., Leckebusch, G. C. and Pinto, J. G. 2009. Extra-tropical cyclones in the present and future climate: a review. *Theor. Appl. Climatol.* **96**, 117–131.
- Uppala, S. M., Kållberg, P. W., Simmons, A. J., Andrae, U., Da Costa Bechtold, V. and co-authors. 2005. The ERA-40 re-analysis. *Q. J. R. Meteorol. Soc.* **131**, 2961–3012.
- Wang, X. L., Swail, V. R. and Zwiers, F. W. 2008. Climatology and changes of extratropical cyclone activity: comparison of ERA40 with NCEP-NCAR reanalysis for 1958–2001. *J. Clim.* **19**, 3145–3166.
- Zhang, X., Zwiers, F. and Li, G. 2004. Monte Carlo experiments on the detection of trends in extreme values. *J. Clim.* **17**, 1945–1952.